The Astrophysical Journal Letters, 743:L15 (6pp), 2011 December 10 doi:10.1088/2041-8205/743/1/L15

FIRST RESULTS FROM THE 3D-HST SURVEY: THE STRIKING DIVERSITY OF MASSIVE GALAXIES AT $z > 1$

Pieter G. van Dokkum[1], Gabriel Brammer[2], Mattia Fumagalli[3], Erica Nelson[1], Marijn Franx[3], Hans-Walter Rix[4], Mariska Kriek[5], Rosalind E. Skelton[1], Shannon Patel[3], Kasper B. Schmidt[4], Rachel Bezanson[1], Fuyan Bian[6], Elisabete da Cunha[4], Dawn K. Erb[7], Xiaohui Fan[6], Natascha Förster Schreiber[8], Garth D. Illingworth[9], Ivo Labbé[3], Britt Lundgren[1], Dan Magee[9], Danilo Marchesini[10], Patrick McCarthy[11], Adam Muzzin[1], Ryan Quadri[11], Charles C. Steidel[12], Tomer Tal[1], David Wake[1], Katherine E. Whitaker[1], and Anna Williams[13]

[1] Department of Astronomy, Yale University, New Haven, CT 06520, USA
[2] European Southern Observatory, Alonso de Córdova 3107, Casilla 19001, Vitacura, Santiago, Chile
[3] Leiden Observatory, Leiden University, Leiden, The Netherlands
[4] Max Planck Institute for Astronomy (MPIA), Königstuhl 17, 69117, Heidelberg, Germany
[5] Harvard-Smithsonian Center for Astrophysics, 60 Garden Street, Cambridge, MA 02138, USA
[6] Steward Observatory, University of Arizona, Tucson, AZ 85721, USA
[7] Department of Physics, University of Wisconsin-Milwaukee, P.O. Box 413, Milwaukee, WI 53201, USA
[8] Max-Planck-Institut für extraterrestrische Physik, Giessenbachstrasse, D-85748 Garching, Germany
[9] Astronomy Department, University of California, Santa Cruz, CA 95064, USA
[10] Physics and Astronomy Department, Tufts University, Robinson Hall, Room 257, Medford, MA 02155, USA
[11] Carnegie Observatories, 813 Santa Barbara Street, Pasadena, CA 91101, USA
[12] California Institute of Technology, MS 249-17, Pasadena, CA 91125, USA
[13] Department of Astronomy, University of Wisconsin-Madison, 475 North Charter Street, Madison, WI 53706, USA

Received 2011 August 30; accepted 2011 October 13; published 2011 November 21

ABSTRACT

We present first results from the 3D-HST program, a near-IR spectroscopic survey performed with the Wide Field Camera 3 (WFC3) on the *HST*. We have used 3D-HST spectra to measure redshifts and Hα equivalent widths ($EW_{H\alpha}$) for a complete, stellar mass-limited sample of 34 galaxies at $1 < z < 1.5$ with $M_{star} > 10^{11}\ M_{\odot}$ in the COSMOS, GOODS, and AEGIS fields. We find that a substantial fraction of massive galaxies at this epoch are forming stars at a high rate: the fraction of galaxies with $EW_{H\alpha} > 10$ Å is 59%, compared to 10% among Sloan Digital Sky Survey galaxies of similar masses at $z = 0.1$. Galaxies with weak Hα emission show absorption lines typical of 2–4 Gyr old stellar populations. The structural parameters of the galaxies, derived from the associated WFC3 F140W imaging data, correlate with the presence of Hα; quiescent galaxies are compact with high Sérsic index and high inferred velocity dispersion, whereas star-forming galaxies are typically large two-armed spiral galaxies, with low Sérsic index. Some of these star-forming galaxies might be progenitors of the most massive S0 and Sa galaxies. Our results challenge the idea that galaxies at fixed mass form a homogeneous population with small scatter in their properties. Instead, we find that massive galaxies form a highly diverse population at $z > 1$, in marked contrast to the local universe.

Key words: cosmology: observations – galaxies: evolution

Online-only material: color figures

1. INTRODUCTION

In the nearby universe galaxies with stellar masses $>10^{11}\ M_{\odot}$ form a homogeneous population, with small scatter in their properties at fixed mass (e.g., Djorgovski & Davis 1987; Blanton et al. 2003; Kauffmann et al. 2003a). This homogeneity is somewhat puzzling in the context of standard models of galaxy formation, as in these models star formation and merging extend to recent epochs (e.g., De Lucia et al. 2006). Models that aim to explain the tight scaling relations of massive galaxies usually invoke "dry" mergers in combination with feedback from active galactic nuclei (AGNs) to prevent gas cooling and star formation (e.g., Croton et al. 2006).

Many studies have measured the properties of massive galaxies at earlier cosmic epochs to better constrain when and how they were formed. Interestingly, it was found that massive galaxies have red rest-frame optical colors at least out to $z \sim 2$ (Bell et al. 2004; Faber et al. 2007; Brammer et al. 2011) and probably beyond (e.g., van Dokkum et al. 2006; Marchesini et al. 2010). Many of these galaxies are compact quiescent galaxies with little or no ongoing star formation (e.g., Daddi et al. 2005; van Dokkum et al. 2008; Damjanov et al. 2009), but at redshifts $z > 1$ a subset of the population has Multiband Imaging Photometer for *Spitzer* 24 μm fluxes and near-IR colors characteristic of dust-obscured star formation (e.g., Papovich et al. 2006; Williams et al. 2010; Brammer et al. 2011). These galaxies masquerade as "dead" red sequence galaxies as they have very similar optical colors but in fact have very high inferred star formation rates.

These apparently star-forming, massive galaxies are progenitors of at least a subset of massive galaxies today. In the nearby universe, strongly star-forming galaxies are typically gas-rich mergers, but several studies have argued that at higher redshift such galaxies more resemble "scaled-up" spiral galaxies than local mergers (Wolf et al. 2005; Muzzin et al. 2010; Elbaz et al. 2011). Interpreting these galaxies, and their relation to the compact quiescent galaxies that exist at the same epoch, has been hampered by a lack of mass-complete samples with homogeneous data at the redshifts of interest. Most existing samples are luminosity-selected rather than mass-selected, are

based on photometric redshifts, lack rest-frame optical morphological information, and/or lack well-calibrated star formation diagnostics.

In this Letter, we construct and study a spectroscopic stellar mass-limited sample of galaxies at $1 < z < 1.5$ in order to quantify the properties of massive galaxies when the universe was ≈5 Gyr old. We use data from the 3D-HST survey (GO-12177, GO-12328), an *HST*/Wide Field Camera 3 (WFC3) Treasury program that provides rest-frame optical spectroscopy and imaging at 0.″13 resolution for thousands of distant galaxies.

2. DATA AND ANALYSIS

The data presented here were obtained in the context of 3D-HST, a 248-orbit *HST* Treasury program in Cycles 18 and 19. 3D-HST is a wide-field, two-orbit depth survey of four (GOODS-South, UDS, AEGIS, and COSMOS) of the CANDELS fields (Grogin et al. 2011; Koekemoer et al. 2011) with the WFC3 G141 grism. The fifth CANDELS field, GOODS-North, was observed by the Cycle 17 program GO-11600 (PI: Weiner); these data are included in the 3D-HST project. The grism provides spatially resolved spectra of all objects in the WFC3 field, covering the wavelength range 1.15 μm–1.65 μm with point-source spectral resolution $R \approx 130$. Accompanying direct imaging in the F140W filter provides the necessary information for wavelength calibration, as well as photometric and morphological information. A typical two-orbit pointing comprises ≈5100 s of integration time in the G141 grism and ≈800 s in the F140W direct imaging filter. In addition to the WFC3 near-IR spectroscopy and imaging, 3D-HST provides parallel Advanced Camera for Surveys (ACS) G800L grism spectroscopy and accompanying F814W imaging in the optical. The survey is described in G. Brammer et al. (2012, in preparation).

The F140W data were reduced using standard procedures for WFC3 imaging data and resampled to a rectangular output grid with 0.″06 pixels. This fine sampling is justified as the four individual exposures in each visit are shifted with respect to each other by an integer + 0.5 pixels in x and y. Spectra were extracted from the grism data using the aXe software (Kümmel et al. 2009), in a similar way as described by van Dokkum & Brammer (2010) and Atek et al. (2010). Details on the specific 3D-HST reduction will be provided in G. Brammer et al. (2012, in preparation). The spectra were combined with photometry at other wavelengths, using publicly available photometric catalogs of Whitaker et al. (2011, COSMOS, AEGIS), Kajisawa et al. (2011, GOODS-North), and Wuyts et al. (2008, GOODS-South). Next, redshifts and emission line fluxes were determined from the combined photometric and spectroscopic data, using a modified version of the EAZY code (Brammer et al. 2008). The slitless spectra require that the template fitting explicitly takes the morphologies of the galaxies into account; therefore, the models are convolved with the F140W direct image averaged in the spatial direction. In our fitting procedure emission lines are "automatically" corrected for underlying stellar absorption. Due to the nature of slitless grism spectroscopy, many spectra are contaminated to some extent by overlapping spectra of neighboring objects. The aXe package provides a quantitative estimate of the contamination as a function of wavelength, which can be subtracted from the spectra.

Stellar masses were determined using the FAST code (Kriek et al. 2009b), using Bruzual & Charlot (2003) models and assuming a Chabrier (2003) stellar initial mass function. We find that the stellar masses differ by <0.05 dex whether or not the spectra are included in the fits. Rest-frame $U-V$ colors were determined directly from the best-fitting spectral energy distributions (SEDs), following the procedures outlined in, e.g., Wolf et al. (2003) and Brammer et al. (2011). Effective radii and Sérsic (1968) indices were determined from the F140W images using GALFIT (Peng et al. 2002), using synthetic point-spread functions and averaging the measurements from each of the dithered exposures. The individual measurements are generally consistent to within <0.05 dex.

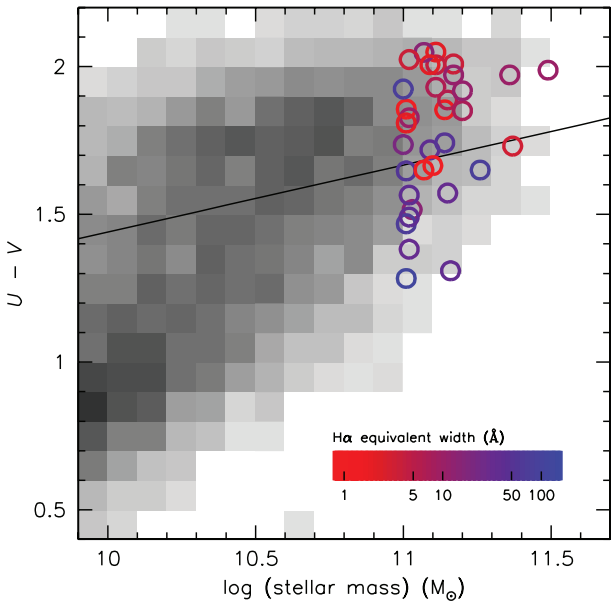

Figure 1. Color–mass relation of galaxies at $1 < z < 1.5$ in the NEWFIRM Medium Band Survey (gray scale). The 3D-HST galaxies are overplotted, color-coded by their Hα equivalent width. The 3D-HST galaxies span a similar range in color as the much larger NMBS sample with $M > 10^{11}\ M_{\odot}$. Star-forming galaxies are typically bluer than galaxies with weak Hα. The line is the separation between blue and red galaxies from Borch et al. (2006), extrapolated to $z = 1.25$.

(A color version of this figure is available in the online journal.)

3. A MASS-LIMITED SPECTROSCOPIC GALAXY SAMPLE AT $z = 1$–1.5

For this initial Letter, we selected galaxies from the 3D-HST survey with stellar masses $M_{\rm star} > 10^{11}\ M_{\odot}$, grism redshifts $1 < z < 1.5$, and low contamination (less than 20% of the measured flux). The only other spectroscopic sample of this kind is the Gemini Deep Deep Survey, which used optical spectroscopy (Abraham et al. 2004). The upper limit on the redshift selection is the highest redshift for which Hα falls in the G141 spectral range.[14] Besides Hα, strong Mg, Na, and TiO absorption features fall in the observed wavelength range, allowing us to measure accurate redshifts for both star-forming and quiescent galaxies. From 68 available *HST* pointings (approximately 50% of the full survey) this selection gives a sample of 34 galaxies. We note that our sample is biased against close pairs, mostly due to the strict contamination criterion. Fifteen of these objects have a spectroscopic redshift previously measured with a ground-based telescope. There is good agreement between the grism redshifts and the spectroscopic redshifts: the 1σ scatter is $0.004 \times (1 + z)$.

In Figure 1, the rest-frame $U-V$ colors of the galaxies in our sample are compared to those of $1 < z < 1.5$ galaxies over

[14] At the resolution of the 3D-HST spectra Hα and [N II] λ6583 cannot be distinguished. Throughout the text "Hα" refers to the combination of these two lines.

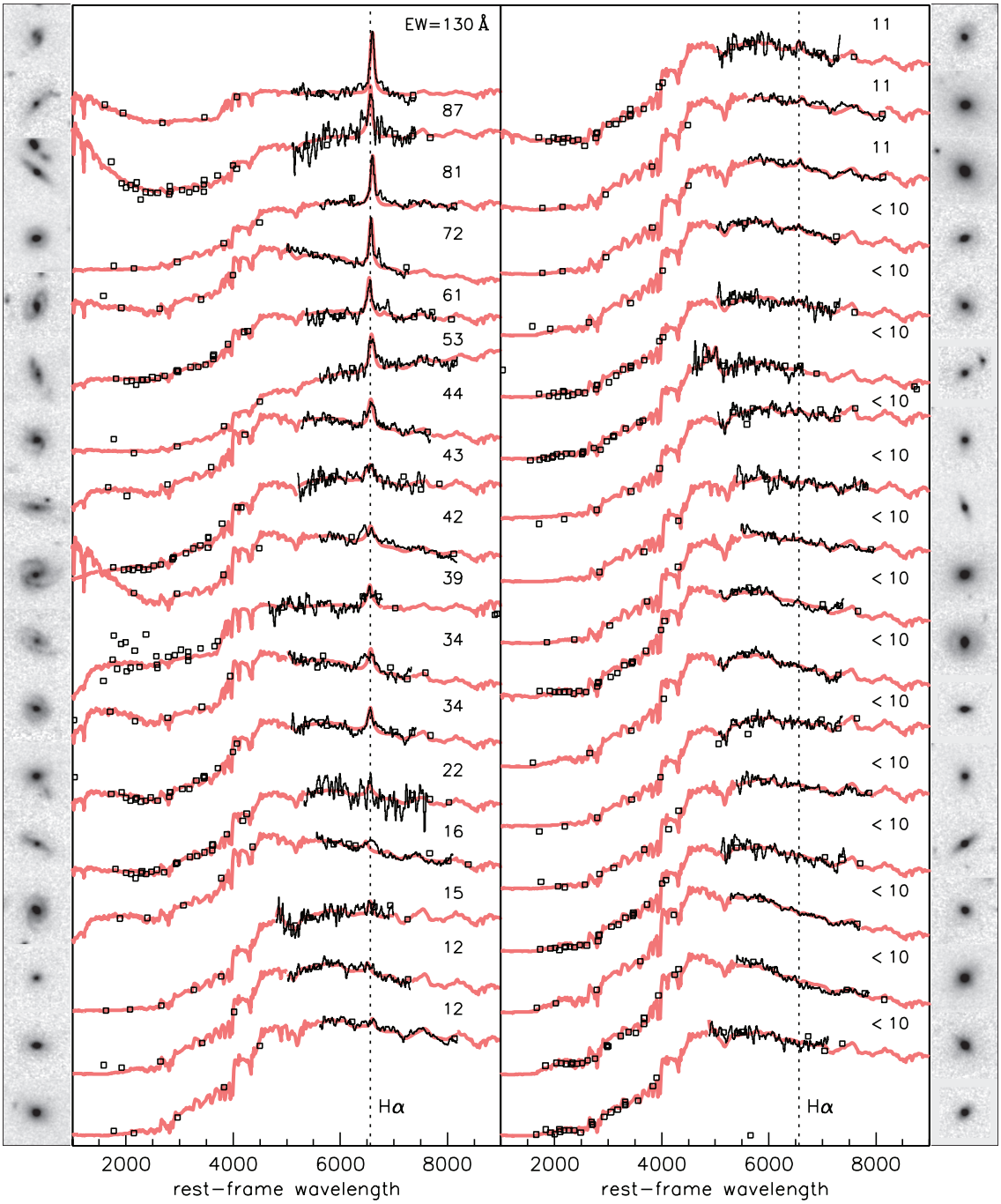

Figure 2. *HST*/WFC3 F140W images and G141 grism spectra of galaxies with $M_{\rm star} > 10^{11}\ M_{\odot}$ and $1 < z < 1.5$. The spectra were averaged in the spatial direction to optimize the S/N and smoothed by a boxcar filter for presentation purposes. The y-axis is in units of F_{λ}; each spectrum was normalized and offset with respect to the others. Squares indicate broad- and medium-band photometry from public catalogs (see the text). The orange spectra are the best-fitting EAZY models (Brammer et al. 2008) for the continuum emission and for Hα. In the grism spectral range the models were convolved with the morphologies of the galaxies to properly model the spectral resolution. The galaxies are ordered by decreasing Hα equivalent width. The spectra are of high quality. The fraction of galaxies with strong Hα emission is much higher than in the nearby universe. Galaxies with strong Hα emission are often two-armed spiral galaxies. Galaxies with weak or undetected Hα typically have an early-type (E, S0, or Sa) morphology.

(A color version of this figure is available in the online journal.)

a large mass range in the NEWFIRM Medium Band Survey (NMBS; Whitaker et al. 2011). The 3D-HST galaxies span a similar range in rest-frame $U-V$ color as massive galaxies in the NMBS. This range is much smaller at $M > 10^{11}\ M_{\odot}$ than at lower masses: all massive galaxies are red compared to blue cloud galaxies at $M \sim 10^{10}\ M_{\odot}$, which have $U - V \sim 0.8$.

4. SPECTRAL FEATURES

The WFC3/G141 spectra and WFC3/F140W images of the galaxies are shown in Figure 2, ordered by decreasing rest-frame Hα equivalent width. We detect Hα emission in 20 galaxies, or in 59% of the sample. The rest-frame equivalent widths for the detected galaxies range from 10 Å to 130 Å. The immediate

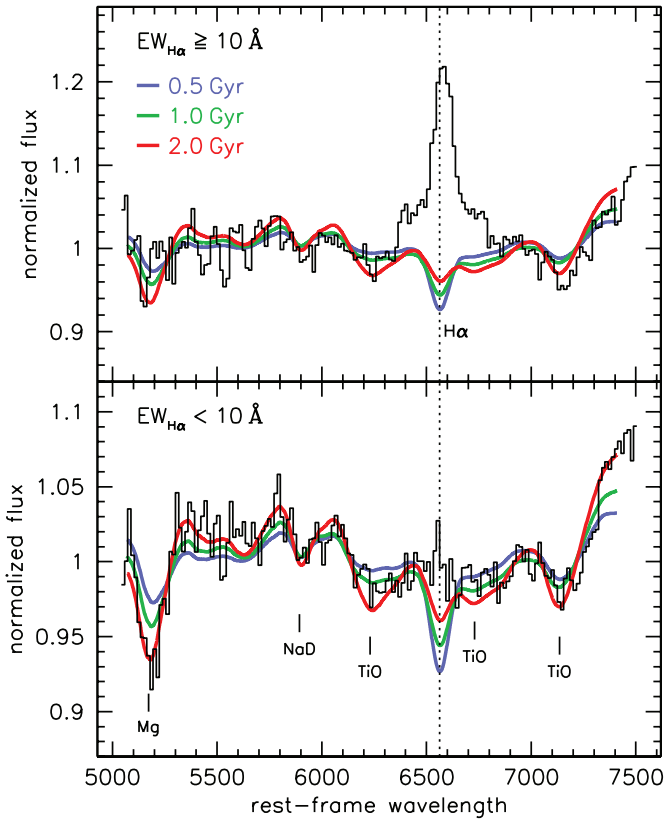

Figure 3. Stacked spectra of the 20 massive galaxies at $1 < z < 1.5$ with $EW_{H\alpha} \geqslant 10$ Å (top panel) and of the 14 galaxies with $EW_{H\alpha} < 10$ Å (bottom panel). The spectra were normalized by dividing them by a second-order polynomial fit. Colored lines are stellar population synthesis models with different ages (see the text), smoothed to the resolution of the stacked spectra. The strong stellar absorption features of the galaxies with weak Hα require luminosity-weighted ages of 2–4 Gyr.

(A color version of this figure is available in the online journal.)

implication is that a substantial fraction of massive galaxies at $1 < z < 1.5$ is likely forming stars. The Hα lines in nearby galaxies in this mass range are substantially weaker: the fraction of galaxies with $EW_{H\alpha} > 10$ Å above the same mass limit at $z = 0.1$ is only ≈10% (Tremonti et al. 2004). Note that the Hα lines are typically broad in the 3D-HST spectra. This is not due to velocity broadening but rather to "morphological broadening:" in slitless spectroscopy spectral features are effectively images of the galaxy in that particular wavelength. This will be discussed further in Section 6.

The galaxies with weak Hα emission have strong stellar absorption features typical of intermediate age stellar populations. This is demonstrated in Figure 3, which compares the averaged rest-frame spectra of galaxies with strong and weak Hα. The stellar absorption features Mg_b, Na D, and several TiO bands are clearly detected in the stacked spectrum of the weak Hα galaxies—for the first time at these redshifts. The colored lines in Figure 3 are stellar population synthesis models of Vazdekis et al. (2010) with metallicity [M/Z] = 0.22 and different ages. The best-fitting age for the galaxies with low star formation is 2 Gyr; models with ages of up to 4 Gyr also provide good fits. We note that this is an average and that the galaxies probably have a range of ages.

As can be seen in Figure 1 the galaxies with strong Hα emission are slightly bluer (by ≈0.3 mag in $U-V$) than the galaxies with weak Hα. The fact that the color difference is relatively small is because the star-forming galaxies have more dust: galaxies with $EW_{H\alpha} < 10$ Å have a mean best-fit $\langle A_V \rangle = 0.5 \pm 0.1$ whereas galaxies with $EW_{H\alpha} > 10$ Å have $\langle A_V \rangle = 1.0 \pm 0.2$ (see also, e.g., Labbé et al. 2005; Papovich et al. 2006; Brammer et al. 2011).

5. STAR FORMATION, STRUCTURE, AND THE DIVERSITY OF MASSIVE GALAXIES

Besides the number of objects with strong Hα emission, a striking aspect of Figure 2 is that the morphologies of the galaxies correlate with the Hα line strength. Massive $1 < z < 1.5$ galaxies with the highest star formation rates tend to be "grand design" spiral galaxies, whereas those with no detected Hα emission tend to be early-type galaxies. This result is qualitatively similar to trends at $z = 0$, although massive galaxies with $EW_{H\alpha} > 10$ Å are rare in the nearby universe (see Section 3).

We quantify this correlation between galaxy structure and star formation rate in the top panel of Figure 4, which shows the relation between $EW_{H\alpha}$ and the Sérsic (1968) index. The Sérsic index is a quantitative measure of galaxy structure and is a proxy for the bulge-to-disk ratio: galaxies dominated by disks have $n \sim 1$ and galaxies dominated by bulges have $n \sim 4$. Splitting the galaxies in two equal bins, the median Sérsic index of the 17 galaxies with $EW_{H\alpha} > 12$ Å is 2.2, whereas it is 4.2 for the 17 galaxies with $EW_{H\alpha} < 12$ Å. According to the Mann–Whitney test this difference is significant at the >99% confidence level. We infer that star formation in massive galaxies at $1 < z < 1.5$ typically takes place in disk-dominated (spiral) galaxies. This result is consistent with recent suggestions that many star-forming galaxies at $z > 1$ are "scaled-up" versions of nearby galaxies (e.g., Elbaz et al. 2011).

The bottom panel of Figure 4 shows the relation between $EW_{H\alpha}$ and the inferred velocity dispersions of the galaxies, which are derived from their stellar masses, effective radii, and Sérsic indices following Bezanson et al. (2011). The inferred dispersions are a measure of the compactness of the stellar components of galaxies as they are proportional to $\sqrt{M/r_e}$ (with a Sérsic-dependent correction factor). Again, there is a clear relation between these quantities: the median inferred dispersion of the half of the sample with the strongest Hα is 174^{+30}_{-25} km s^{-1}, whereas it is 299^{+51}_{-43} km s^{-1} for the galaxies with the weakest Hα. The relation between $EW_{H\alpha}$ and dispersion has much smaller scatter than the relations of $EW_{H\alpha}$ with effective radius and mass separately. The trend in Figure 4 is qualitatively consistent with the relation between estimated specific star formation rate (SSFR) and inferred dispersion found by Franx et al. (2008).

Figure 4 showcases the large variety of galaxies. The range in $EW_{H\alpha}$ among massive galaxies with *detected* Hα is a factor of 12, and it is obviously even larger when undetected galaxies are taken into account (see Figure 3). The structure and morphologies of galaxies also show a large range, going from large spiral galaxies with high $EW_{H\alpha}$ to compact early-type galaxies with low $EW_{H\alpha}$. The Sérsic indices span the full range between disk-to-bulge-dominated values ($n \sim 1$ to $n \sim 4$) and the inferred dispersions range from $\lesssim$150 km s^{-1} to $\gtrsim$400 km s^{-1}.

6. DISCUSSION

We have shown that the 3D-HST Treasury program is providing high-quality near-IR spectroscopy and accompanying imaging for galaxies in the crucial epoch $1 < z < 3$, when the

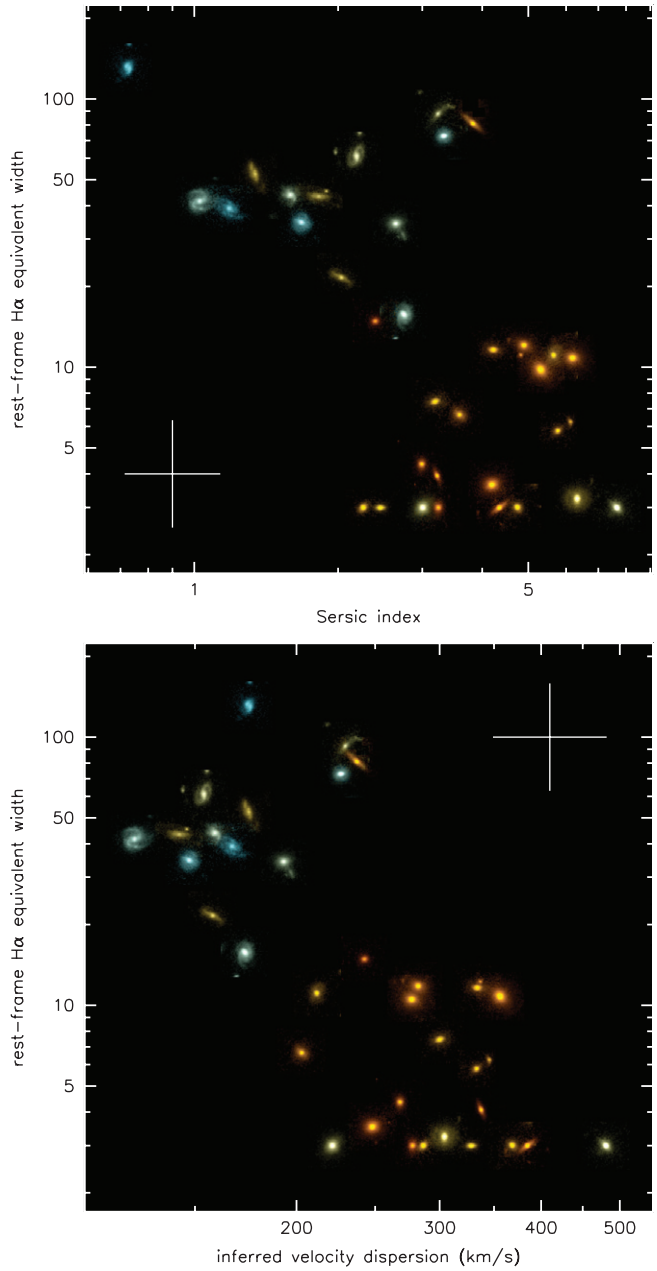

Figure 4. Top panel: relation between $EW_{H\alpha}$, Sérsic index, and morphology. The F140W images are color-coded according to their average $U-V$ color. Bottom panel: relation between $EW_{H\alpha}$, velocity dispersion, and morphology. The velocity dispersions were inferred from the stellar masses, effective radii, and Sérsic n values of the galaxies. The error bars denote the typical uncertainties, as determined from a combination of formal errors and varying the fitting methodology. Sérsic index, velocity dispersion, and morphology all correlate with the strength of Hα. All these parameters span large ranges: massive galaxies exhibit a striking diversity at $1 < z < 1.5$, ranging from large star-forming spiral galaxies to compact quiescent galaxies.

(A color version of this figure is available in the online journal.)

cosmic star formation rate peaked (e.g., Bouwens et al. 2007). In this first Letter we focused on a stellar mass-limited sample of 34 galaxies at $z = 1$–1.5 to study the properties of massive galaxies when the universe was 4–6 Gyr old. This is the first study of the Hα emission and rest-frame optical morphologies of a complete, mass-limited galaxy sample at $z > 1$.

The most striking result of our study is the diversity of the spectra and structure of massive galaxies at $z > 1$: a large fraction has strong Hα emission, whereas others have absorption features characteristic of relatively old stellar populations. Similarly, the morphologies, Sérsic indices, and implied velocity dispersions show a large range. These results are broadly consistent with previous studies that were based on photometric redshifts, the SED shapes of galaxies, and/or imaging of lower quality (e.g., Franx et al. 2008; Williams et al. 2010; Wuyts et al. 2011b; Weinzirl et al. 2011). The simplest interpretation is that at $z > 1$ we are entering the epoch when massive galaxies were undergoing rapid evolution. Specifically, the star-forming disks may be progenitors of some of today's most massive S0 and Sa galaxies.

Noeske et al. (2007) suggested that the star formation rates of galaxies are tightly coupled to their mass and redshift, and it is interesting to compare the range in $EW_{H\alpha}$ in our sample to the scatter in their "star formation main sequence." At fixed mass Noeske et al. (2007) find a 68% range in star formation rates of a factor of ∼4 (among galaxies with clear signs of star formation); if we limit the sample to the central 68% of the distribution of galaxies with $EW_{H\alpha} > 10$ Å we find a larger range of a factor of six. More to the point, within our sample the scatter in $EW_{H\alpha}$ can be significantly reduced by considering the structure of the galaxies. The 68% range in $EW_{H\alpha}$ among the 11 galaxies with inferred $\sigma < 200$ km s^{-1} is only a factor of 1.7. We therefore follow earlier work in suggesting that velocity dispersion (or surface density) is a more fundamental parameter than mass in determining the properties of galaxies (see, e.g., Kauffmann et al. 2003b; Franx et al. 2008; Bezanson et al. 2011).

The growth rate of the star-forming galaxies is substantial; using standard prescriptions to correct for extinction toward H II regions (Calzetti et al. 2000; Wuyts et al. 2011a), we find a median stellar mass increase due to star formation of ∼50% per Gyr for the galaxies with $EW_{H\alpha} > 10$ Å. An important question is *where* in the galaxies the star formation is occurring, that is, which structural component of massive galaxies is in the process of formation at $1 < z < 1.5$. Due to the nature of grism spectroscopy the 3D-HST data provide two-dimensional emission line maps at the spatial resolution of *HST*. Two examples are shown in Figure 5: in these galaxies the star formation appears to trace the spiral arms, similar to spiral galaxies in the nearby universe. A quantitative analysis of the spatial extent of the emission line gas is beyond the scope of this Letter, but we note here that in cases such as those shown in Figure 5 the spatial extent of the Hα emission rules out dominant contributions from active nuclei to the integrated line fluxes.

A key open question is what drives the diversity of massive galaxies at $z > 1$. At fixed stellar mass, we see large, star-forming spiral galaxies and very compact galaxies in which star formation has apparently ceased. If AGN feedback is responsible for shutting off star formation in massive galaxies it is clearly more effective in some galaxies than in others. It may be that AGN feedback correlates with black hole mass, which correlates better with velocity dispersion than with stellar mass (e.g., Magorrian et al. 1998). It will also be interesting to study correlations with other parameters, such as the environment, at fixed stellar mass and at fixed (inferred) velocity dispersion. Finally, it will be important to extend this study to lower masses and to higher redshifts. Star-forming galaxies that have been studied at $z \gtrsim 2$ tend to have higher $EW_{H\alpha}$ and also more irregular morphologies than the galaxies studied here (e.g., Erb et al. 2006; Kriek et al. 2009a; Förster Schreiber et al. 2011), and it will be interesting to see whether a broader selection of galaxies would only increase the dynamic range in Figure 4 or (also) increase the scatter.

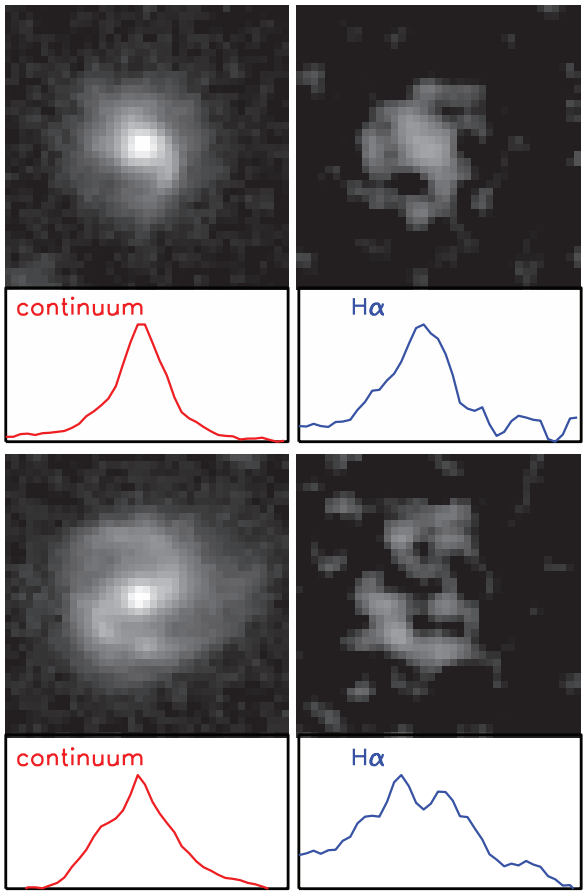

Figure 5. Spatial distribution of continuum emission in the F140W filter compared to the spatial distribution of the Hα line emitting gas. The Hα images were made by subtracting a polynomial fit from the two-dimensional G141 grism spectra. The boxes are $4\farcs7 \times 4\farcs7$, or 39 kpc $\times$ 39 kpc. The line profiles show the flux distributions averaged along the y-axis. The line emission in these particular galaxies is extended, and the galaxies are building up their disks. We also find galaxies with more compact Hα distributions.

(A color version of this figure is available in the online journal.)

Such studies will be possible with the full 3D-HST data set, which will provide WFC3 and ACS spectroscopy and imaging of large samples of galaxies at $z > 1$. Combined with deep imaging from the CANDELS project and the wide array of ancillary data in the survey fields, 3D-HST will provide a qualitatively new way of surveying the heyday of galaxy formation at $1 < z < 3$.

REFERENCES

Abraham, R. G., Glazebrook, K., McCarthy, P. J., et al. 2004, AJ, 127, 2455
Atek, H., Malkan, M., McCarthy, P., et al. 2010, ApJ, 723, 104
Bell, E. F., Wolf, C., Meisenheimer, K., et al. 2004, ApJ, 608, 752
Bezanson, R., van Dokkum, P. G., Franx, M., et al. 2011, ApJ, 737, L31
Blanton, M. R., Hogg, D. W., Bahcall, N. A., et al. 2003, ApJ, 594, 186
Borch, A., Meisenheimer, K., Bell, K. F., et al. 2006, A&A, 453, 869
Bouwens, R. J., Illingworth, G. D., Franx, M., & Ford, H. 2007, ApJ, 670, 928
Brammer, G. B., van Dokkum, P. G., & Coppi, P. 2008, ApJ, 686, 1503
Brammer, G. B., Whitaker, K. E., van Dokkum, P. G., et al. 2011, ApJ, 739, 24
Bruzual, G., & Charlot, S. 2003, MNRAS, 344, 1000
Calzetti, D., Armus, L., Bohlin, R. C., et al. 2000, ApJ, 533, 682
Chabrier, G. 2003, PASP, 115, 763
Croton, D. J., Springel, V., White, S. D. M., et al. 2006, MNRAS, 365, 11
Daddi, E., Renzini, A., Pirzkal, N., et al. 2005, ApJ, 626, 680
Damjanov, I., McCarthy, P. J., Abraham, R. G., et al. 2009, ApJ, 695, 101
De Lucia, G., Springel, V., White, S. D. M., Croton, D., & Kauffmann, G. 2006, MNRAS, 366, 499
Djorgovski, S., & Davis, M. 1987, ApJ, 313, 59
Elbaz, D., Dickinson, M., Hwang, H. S., et al. 2011, A&A, 533, 119
Erb, D. K., Steidel, C. C., Shapley, A. E., et al. 2006, ApJ, 647, 128
Faber, S. M., Willmer, C. N. A., Wolf, C., et al. 2007, ApJ, 665, 265
Förster Schreiber, N. M., Shapley, A. E., Erb, D. K., et al. 2011, ApJ, 731, 65
Franx, M., van Dokkum, P. G., Schreiber, N. M. F., et al. 2008, ApJ, 688, 770
Grogin, N. A., Kocevski, D. D., Faber, S. M., et al. 2011, ApJS, submitted (arXiv:1105.3753)
Kajisawa, M., Ichikawa, T., Tanaka, I., et al. 2011, PASJ, 63, 379
Kauffmann, G., Heckman, T. M., White, S. D. M., et al. 2003a, MNRAS, 341, 33
Kauffmann, G., Heckman, T. M., White, S. D. M., et al. 2003b, MNRAS, 341, 54
Koekemoer, A. M., Faber, S. M., Ferguson, H. C., et al. 2011, ApJS, submitted (arXiv:1105.3754)
Kriek, M., van Dokkum, P. G., Franx, M., Illingworth, G. D., & Magee, D. K. 2009a, ApJ, 705, L71
Kriek, M., van Dokkum, P. G., Labbé, I., et al. 2009b, ApJ, 700, 221
Kümmel, M., Walsh, J. R., Pirzkal, N., Kuntschner, H., & Pasquali, A. 2009, PASP, 121, 59
Labbé, I., Huang, J., Franx, M., et al. 2005, ApJ, 624, L81
Magorrian, J., Tremaine, S., Richstone, D., et al. 1998, AJ, 115, 2285
Marchesini, D., Whitaker, K. E., Brammer, G., et al. 2010, ApJ, 725, 1277
Muzzin, A., van Dokkum, P., Kriek, M., et al. 2010, ApJ, 725, 742
Noeske, K. G., Weiner, B. J., Faber, S. M., et al. 2007, ApJ, 660, L43
Papovich, C., Moustakas, L. A., Dickinson, M., et al. 2006, ApJ, 640, 92
Peng, C. Y., Ho, L. C., Impey, C. D., & Rix, H.-W. 2002, AJ, 124, 266
Sérsic, J. L. 1968, Atlas de galaxias australes (Cordoba: Observatorio Astronomico)
Tremonti, C. A., Heckman, T. M., Kauffmann, G., et al. 2004, ApJ, 613, 898
van Dokkum, P. G., & Brammer, G. 2010, ApJ, 718, L73
van Dokkum, P. G., Franx, M., Kriek, M., et al. 2008, ApJ, 677, L5
van Dokkum, P. G., Quadri, R., Marchesini, D., et al. 2006, ApJ, 638, L59
Vazdekis, A., Sánchez-Blázquez, P., Falcón-Barroso, J., et al. 2010, MNRAS, 404, 1639
Weinzirl, T., Jogee, S., Conselice, C. J., et al. 2011, ApJ, in press (arXiv:1107.2591)
Whitaker, K. E., Labbé, I., van Dokkum, P. G., et al. 2011, ApJ, 735, 86
Williams, R. J., Quadri, R. F., Franx, M., et al. 2010, ApJ, 713, 738
Wolf, C., Bell, E. F., McIntosh, D. H., et al. 2005, ApJ, 630, 771
Wolf, C., Meisenheimer, K., Rix, H.-W., et al. 2003, A&A, 401, 73
Wuyts, S., Forster Schreiber, N. M., Lutz, D., et al. 2011a, ApJ, 738, 106
Wuyts, S., Forster Schreiber, N. M., van der Wel, A., et al. 2011b, ApJ, submitted (arXiv:1107.0317)
Wuyts, S., Labbé, I., Schreiber, N. M. F., et al. 2008, ApJ, 682, 985